INL/JOU-21-63866-Revision-0

Solid-State Phase Transitions of Two Quaternary Metallic Fuel Alloys (U-2.5Mo-2.5Ti-5.0Zr and U-1.5Mo-1.5Ti-7.0Zr in wt. %)

November 2021

Weiqian Zhou, Huali Wu, Yi Xie, Jinsuo Zhang, Michael T Benson

Changing the World's Energy Future

Idaho National Laboratory

INL is a U.S. Department of Energy National Laboratory operated by Battelle Energy Alliance, LLC

INL/JOU-21-63866-Revision-0

Solid-State Phase Transitions of Two Quaternary Metallic Fuel Alloys (U-2.5Mo-2.5Ti-5.0Zr and U-1.5Mo-1.5Ti-7.0Zr in wt. %)

Weiqian Zhou, Huali Wu, Yi Xie, Jinsuo Zhang, Michael T Benson

November 2021

Idaho National Laboratory
Idaho Falls, Idaho 83415

http://www.inl.gov

Prepared for the
U.S. Department of Energy
Under DOE Idaho Operations Office
Contract DE-AC07-05ID14517

Solid-State Phase Transitions of Two Quaternary Metallic Fuel Alloys (U-2.5Mo-2.5Ti-5.0Zr and U-1.5Mo-1.5Ti-7.0Zr in wt. %)

Weiqian Zhuo[a], Huali Wu[a], Yi Xie[b], Michael T. Benson[b], Jinsuo Zhang[a,*],

[a] Nuclear Engineering Program, Department of Mechanical Engineering, Virginia Tech, Blacksburg, Virginia 24061, USA
[b] Idaho National Laboratory, P.O. Box 1625, Idaho Falls, ID 83415, USA
*Corresponding author, Email: zjinsuo5@vt.edu

Abstract

This study focuses on the solid-state phase transitions of two quaternary fuel alloys for fast reactors: U-1.5Mo-1.5Ti-7.0Zr (U-MT7Z) and U-2.5Mo-2.5Ti-5.0Zr (U-MT5Z). The phase transitions were determined by differential scanning calorimetry (DSC), X-ray powder diffraction (XRD), and scanning electron microscopy/energy dispersive X-ray spectroscopy (SEM/EDS). To identify the high temperature phases, the alloys were annealed at 873K, 948K, 1023K, and 1123K (all under 72 hours). Combining those characterizations, the phase transitions are determined. In U-MT7Z, there is one phase transition observed, and it is ascribed to $\alpha + U_2Ti \rightarrow \gamma$ transition. In U-MT5Z, two transitions are found. The first transition is $\alpha \rightarrow \gamma$, while the second is $U_2Ti \rightarrow \gamma$. The γ phase onset temperature of U-MT5Z is lower than that of U-MT7Z due to the higher Mo content.

Keywords: Quaternary uranium alloy, phase transition, DSC, XRD, SEM/EDS

1. Introduction

Alloys of uranium, specifically U-10Zr and U-10Mo (both in wt. %), are important and extensively studied metallic fuel forms. U-10Zr has the advantage of high solidus/liquidus temperatures, ~1533K and 1633K, respectively, providing a safety buffer over the melting point of pure U (1408K). The disadvantage of U-10Zr is the redistribution of Zr that occurs during irradiation [1]. The mid-radial region loses Zr and becomes essentially pure U, while the center of the fuel pin becomes concentrated in Zr. Due to the temperature gradient present in the fuel, the phases present transition from α-U and UZr_2 at the fuel periphery, and then to (U, Zr)-γ phase in the center. U-10Mo remains evenly dispersed in the fuel and does not redistribute during irradiation, but there is no advantage in melting point, as the solidus/liquidus temperatures are roughly the same as the melting point for pure U. The advantage of U-10Mo is the low onset temperature of the γ phase, which has isotropic swelling, and also allows the fuel pin to be in the same phase throughout, regardless of the temperature gradient. However, one disadvantage of U-10Mo is that it causes more fuel-cladding chemical interactions (FCCIs) as compared to U-10Zr under similar irradiation condition [2].

By combining these systems, the advantages can potentially be maintained while minimizing the disadvantages. Mariani proposed an alloy containing Mo, Zr, Ti with U (or quaternary UMTZ alloy) [3, 4], with the expectation of decreasing the γ phase onset temperature (by Mo) and increasing the solidus/liquidus temperatures (by Zr and Ti) over that of pure uranium [3, 4, 5]. A low γ phase onset temperature will be beneficial due to the isotropic swelling in this cubic phase [4,6]. For pure uranium, the γ phase onset temperature is 1049K. This temperature can be reduced by alloying uranium with other elements such as Mo, Nb, Zr, or Ti, according to the binary phase diagrams [7, 8, 9, 10]. For example, in the U-rich region containing around 70 at. % uranium, the γ onset temperature is 828K for U-Mo [7], 947K for U-Nb [8], 890K for U-Zr [9], and 996K for U-Ti [10]. The γ phase onset temperatures are lower than that of pure uranium, with Mo being the most effective element in this regard. Hence, the γ phase onset temperatures for UMTZ alloy should be investigated. To determine the γ phase onset temperature, an investigation of the phase transitions is needed. To date, the UMTZ system has undergone relatively little investigation, and the phase transitions were not well characterized. Some preliminary investigations have been performed on the 90.0U-5.0Mo-4.3Ti-0.7Zr (wt. %) alloy [2, 5, 11, 12]. Constituent redistribution was not observed in this alloy, but there was significant fuel-cladding chemical interaction (FCCI) during irradiation, primarily due to the low Zr content and high Mo content. Mo-Fe interactions are a known concern when combining a fuel alloy containing Mo with a Fe-based cladding. To minimize FCCI due to Mo, the Mo content in the fuel has to be minimized, while still having enough Mo to produce the desired effect. Based on the previous results, two alloys with lower Mo contents, i.e., 90.0U-2.5Mo-2.5Ti-5Zr (wt. %) and 90.0U-1.5Mo-1.5Ti-7Zr (wt. %), have been prepared and characterized [13], however, the phase transitions were not determined in the study.

This work is a continuation of the previous microstructural study [13] focusing on the solid-state phase transitions for the two UMTZ alloys (as listed in Table 1). In both alloys, the content of U is 90 wt. % and the contents of Mo and Ti are the same (2.5 wt. % or 1.5 wt. %). For simplicity, the weight percent of Zr, either 5 or 7, is used to name the alloys, i.e. U-MT5Z and U-MT7Z.

Because the available studies indicate that a high Mo content (e.g. U-10Mo or U-5.0Mo-4.3Ti-0.7Zr, wt. %) will lead to significant FCCI [5, 2, 11], only alloys with low Mo content are being considered in this investigation.

Table 1. Targeted alloy compositions

Alloy	wt. %	at. %
U-MT5Z	90.0U-2.5Mo-2.5Ti-5.0Zr	74.0U-5.1Mo-10.2Ti-10.7Zr
U-MT7Z	90.0U-1.5Mo-1.5Ti-7.0Zr	75.4U-3.1Mo-6.2Ti-15.3Zr

2. Materials and Experiments

2.1 Materials

All materials except U were obtained from Alfa Aesar and used as received. All casting operations were carried out with an arc-melter in an argon atmosphere glovebox with high purity argon as a cover gas. The appropriate amount of U, Mo, Ti, and Zr was arc-melted together in two steps. The first step was melting Mo, Ti, and Zr together, followed by the addition of U. After each step, the cast button was flipped and re-melted three times to ensure homogeneity. The resulting buttons of U-Mo-Ti-Zr were cast into 5 mm diameter pins using a drop casting technique. Then, a thin sample pellet was cut from each pin and used for the study.

2.2 Experimental details

The phase transitions were characterized in the following manner. Firstly, the phase transition peaks of the alloys were determined by DSC. The DSC tests were performed on as-cast samples with an effective temperature range from 473K to 1123K. During each test, two heating/cooling cycles were performed. The 1st cycle was to remove the thermal history of the sample and the 2nd cycle was used to present the results. The tests were performed five times for each alloy, and a fresh sample was employed for each test. In this step, the temperautures of the phase transitions were obtained, but the phases were still not known. So the second step was to identify the starting phases and the phases at high temperatures. To identify the starting transition phases, the DSC post-test samples were used. There were two cycles in each DSC run, since the data of the 2nd cycle was used (the 1st cycle was not used), the starting phases present at the beginning of the 2nd cycle should be identified. The starting phases present at the beginning of the 2nd cycle were the phases that cooled down from the 1st cycle. In each DSC run, the cooling process was the same in each cycle (cooled down with furnace, with the cooling rate estimated to be around 18K /min), so the phases were the same either cooled down from 1st cycle or 2nd cycle. In other words, the phases present in the DSC post-test sample were the starting phases of the DSC test. To identify the phases at high temperatures, the annealed alloys were used. The annealing conditions were 873K, 948K, 1023K, and 1123K with the annealing time of 72h for all cases. The DSC post-test samples and the annealed samples were characterized by XRD and SEM/EDS.

2.2.1 Sample preparation

Prior to the DSC, XRD, and SEM/EDS characterizations, the samples were prepared according to the details as listed in Table 2. All characterizations were performed without any mountings on the samples.

Table 2. Sample preparation details for XRD, SEM, and DSC Characterizations.

Characterization	Thickness	Mass	Sample surface preparation method
DSC	< 1 mm	80 – 120 mg	The surface was ground using SiC sandpapers (with grit size 400, 600).
XRD	1 - 2 mm*	300 – 700 mg*	Same as for DSC.
SEM/EDS	1 - 2 mm*	300 – 700 mg*	The surface was ground using SiC sandpapers (with grit size 600, 800, 1000, 1200) followed by polishing using polycrystalline diamond suspensions (1 μm).

* The parameter is for the annealed samples.

2.2.2 Experiments and characterizations

2.2.2.1 DSC

The DSC tests were carried out in a TA Instruments SDT-Q600. Ultra-high purity argon (oxygen < 10 ppb) with a flow rate of 100 mL/min was used to purge the chamber of the DSC. Alumina cups were used for all the DSC tests. To calibrate the DSC, a three-point temperature calibration was performed using the standard materials zinc (purity 99.995 %, melting point 692.68K [14]), aluminum (purity 99.97 %, melting point 933.47K [14]), and silver (purity 99.999 %, melting point 1234.93K [14]). To determine the phase transition temperature, the analysis was conducted in the following steps by using the software Origin 2020. First, the DSC data with the peak(s) are selected and a baseline subtraction was performed. To determine the phase transition temperature, the peak was fitted by the Asymmetric Double Sigmoidal (Asym2sig) function. The Asym2sig function was used if the phase transition peak was not symmetric [15]. The quality of the fitting was determined by R-square (coefficient of determination), with the R-square ≥ 0.996 as the criteria. Then, the fitted peak was analyzed using the "onset for peak" module in Origin to determine the onset temperature (T_{onset}), extrapolated temperature (T_{ext}), and endset temperature (T_{endset}). The onset temperature is the intersection point of the extrapolated baseline and the inflectional tangent at the beginning of the peak. The extrapolated temperature is the intersection point of the inflectional tangent at the beginning of the peak and the inflectional tangent at the end of the peak. The endset temperature is the intersection point of the extrapolated baseline and the inflectional tangent at the end of the peak (see Figure 2 as an example). In the case of DSC analysis, the onset temperature of the peak indicates the start of the phase transition. The onset temperature is generally used as the phase transition temperature because it is less dependent on the heating rate and sample mass [16, 17].

To verify the DSC in the temperature range of interest for these specific alloys, tests were performed using the same U feedstock as used in the alloy fabrication. The feedstock is 99.782 wt. % U, based on ICP-MS chemical analysis. Samples of U were run with three heating rates, 5K/min, 10K/min, and 15K/min. Three runs were performed for each heating rate.

Representative DSC curves are shown in Figure 1, and the averaged onset tempeartures (T_o) and standard deviations (SD) are listed in Table 3. The onset temperatures obtained from 5K/min heating rate are the closest to the literature values. For this reason, the heating rate of 5K/min was chosen in this study.

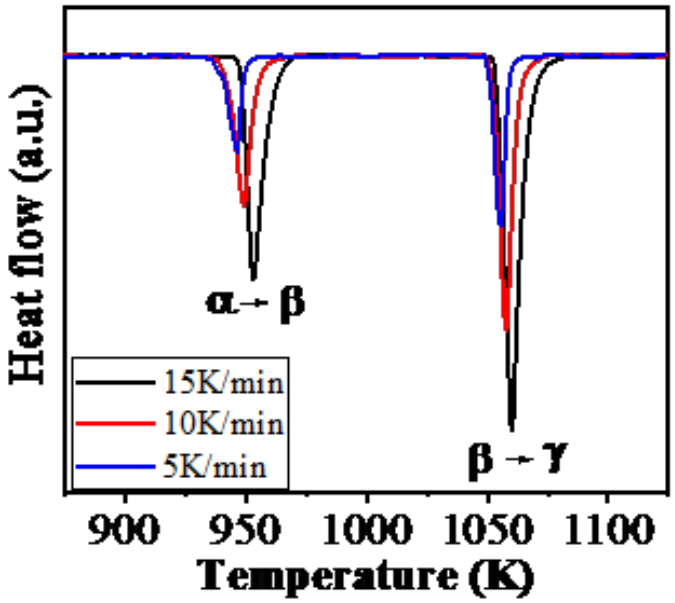

Figure 1. Representative DSC curves of pure uranium with three different heating rates.

Table 3. Peak onset temperatures for pure uranium.

	α→ β		β→ γ	
	T_o (K)	Deviation*	T_o (K)	Deviation*
5K/min	940.09 ± 0.18	-0.11%	1050.69 ± 0.59	0.15%
10K/min	942.68 ± 0.90	0.16%	1052.57 ± 1.02	0.33%
15K /min	947.87± 1.73	0.71%	1054.49 ± 2.63	0.51%
Literature value [7]	941.15	-	1049.15	-

*Deviation from literature value.

2.2.2.2 Annealing tests

The samples were annealed in a furnace inside an argon-filled environment. The samples were annealed at four different temperatures, i.e. 873K, 948K, 1023K, and 1123K, with an annealing time of 72 hours for all cases. These temperatures are independent of each other, i.e. the sample annealed at 948K was not annealed at 873K prior. After annealing, the alloys were immediately placed in Si-based oil for 2 minutes to quench.

2.2.2.3 XRD

The samples were characterized by XRD for the phase structure identification. A PANalytical X'Pert Empyrean XRD with copper source was used for the analysis. The XRD instrument was calibrated with a silicon standard sample. In each XRD scan, the step size was 0.007162°/step, and the scan rate was 1°/min.

2.2.2.4 SEM/EDS

The microstructure analysis was performed on a FEI Quanta 600 FEG SEM equipped with a Bruker energy dispersive spectrometer. The SEM was operated at an accelerating voltage of 20 kV and a spot size of 5. Spectra were collected over the energy range of 0-10 keV. Energy calibration was conducted by referencing to the L-α peak and K-α peak from a standard Cu disk. The peaks of the U M-series, Zr L series, Mo L series, and Ti L series were used for the EDS point quantification in Esprit 1.9 software. Note that the calibration was performed using a Cu disk, but this calibration may not be sufficient when detecting heavier elements like U, especially when presenting the quantitative data from EDS point scans.

3. Results

3.1 U-MT7Z

3.1.1 DSC

An example of the DSC curve on U-MT7Z is shown in Figure 2a. There is one phase transition found. A representative example for the quantification of the peak data for the single peak in U-MT7Z is shown in Figure 2b. The experimental data with the temperature range between 773K and 1073K are used. The fitted curve is in good agreement with the experimental data. The peak data of T_{onset}, T_{ext}, and T_{endset} are subsequently determined to be 893.1K, 919.5K, and 927.8K, respectively. Other curves were analyzed using the same procedure, and the averaged data with the standard deviation are obtained. The values of T_{onset}, T_{ext}, and T_{endset} were determined to be 894.3 ± 3.7K, 918.4 ± 2.1, and 926.5 ± 1.9K, respectively.

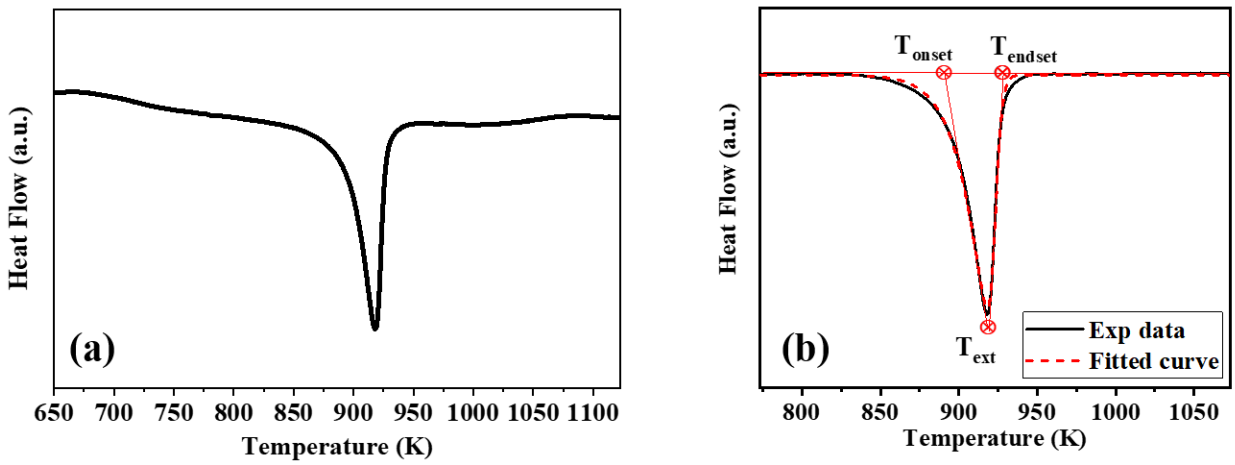

Figure 2. DSC analysis for U-MT7Z alloy: (a) an example of the DSC curve, (b) depiction of the peak.

3.1.2 XRD

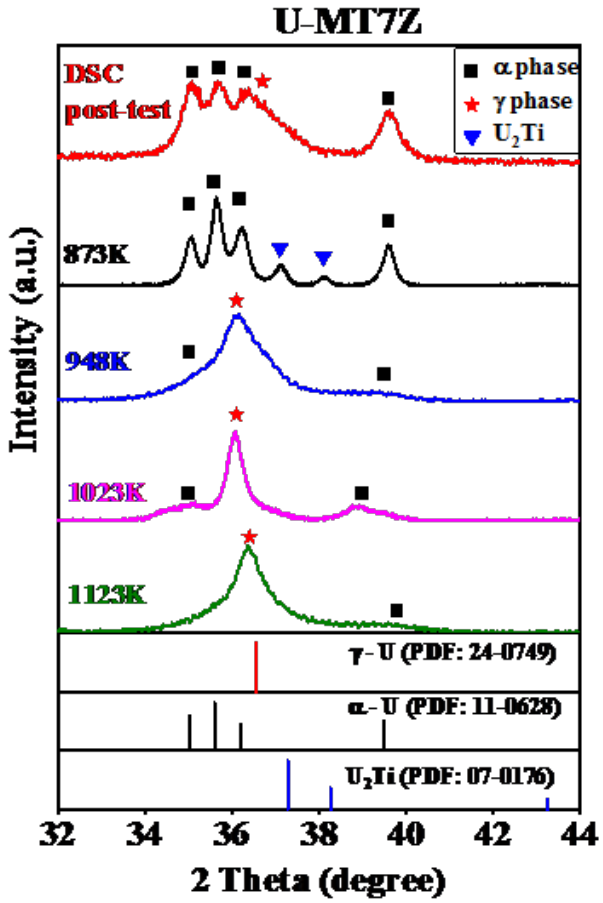

Figure 3. XRD results for U-MT7Z.

The XRD results for U-MT7Z are shown in Figure 3. The high intensity peaks between $2\theta = 32°$ and 44° are indicative of the phases present, so that is the region shown in Figure 3 with reference spectra for γ-U, α-U, and U_2Ti shown at the bottom. The DSC post-test sample is comprised of α and γ phases. At 873K, α-U and U_2Ti are found. In samples annealed at 948K, 1023K, and 1123K, α and γ phases are present.

It is worth mentioning that there are different variants of α-U and γ-U phases that can exist in a uranium alloy (e.g., α', α'', γ^0, γ^s etc.) [18,19,20]. These phases are metastable and may be present when quenching the alloy from high temperature. The results here showing the peaks are broad, except for the sample annealed at 873K, thus it is not able to distinguish the exact phase in the sample. For example, the α phase marked in the DSC post-test sample or the sample annealed at 948K /1023K /1123K could be α-U (orthorhombic), α'(orthorhombic), or α'' (monoclinic) but it is not differentiable due to the diffuse peak. Thus, the terms "α phase" or "γ phase" will be used except for the sample annealed at 873K. In the sample annealed at 873K, the peaks are distinguishable, hence, it is determined to be α-U phase.

3.1.2 SEM/EDS

The representative microstructures under backscattered electrons (BSE) are shown in Figure 4 to Figure 8. Different phases were found and marked in the images, and the averaged compositional data are listed in Table 4. The averaged composition was obtained via three EDS points (the points were at least 10 μm away from each other) on the same phase, and the selected points were placed as close to the center of the phase as possible. Given the small size of the precipitates, the electron beam interaction volume will detect extraneous elements outside the region of interest, complicating the composition analysis. The EDS resolution was estimated to be 1 μm, so precipitates with a size less than 1 μm were excluded from the analysis. The EDS error is estimated up to ± 5 at.%, primary depending on the size of the phase. The smaller phase size attributes to a higher EDS error due to the interaction volume. For example, while quantifying the phase with several microns (bulk phase), the error is generally around ± 1 at. %. However, while quantifying the black participates, the error could be up to ± 5 at.%, as the size is around 1 um or less.

The microstructure of the DSC post-test sample is shown in Figure 4. The bright matrix is a U-rich phase, and the black precipitates are Zr-rich phases, as marked in Figure 4b. The cellular microstructure is observed at the grain boundaries, as shown in Figure 4c. This should be due to the so-called cellular reaction. In U-Mo or U-Mo-Zr alloys, cellular reactions were observed, resulting in the decomposition of γ-phase into α-lamellae and γ-lamellae at the grain boundaries [21,22,23].

For the sample annealed at 873K (Figure 5), there are four phases found:

1. α-U phase (bright). The EDS analysis indicates pure U, and this is supported by XRD (Figure 3).
2. U_2Ti (light grey). The EDS analysis indicates a U:Ti ratio close to 2:1. Combined with the XRD data, this phase is identified as U_2Ti.
3. U-Zr compound (dark grey). These areas mainly contain U and Zr with some Mo and Ti. The phase is composed of about equal amounts of U and Zr, although the phase is likely UZr_2, with excess U detected due to interaction volume. UZr_2 was not observed in XRD, though it is very difficult to detect due to peak overlap with α-U [24, 25].
4. Zr-rich phase (black). Precipitates with a high Zr content were detected according to the EDS point data. This phase is commonly found in U-Zr or U-Pu-Zr alloys [26, 27, 28, 29, 30], possibly formed by impurity such as C, O, N during the fabrication [29]. This could be α-Zr, but such phases are difficult to identify under XRD due to the small amount and/or they are overlapped with α-U [31].

For the samples annealed at 948K (Figure 6), 1023K (Figure 7), and 1123K (Figure 8), regions with two different contrasts, i.e., bright and dark are observed. The microstructure is significantly simplified from the complex microstructure observed for the sample annealed at 873K, indicating the transition to a γ phase incorporating U, Mo, Ti, and Zr. In all cases, the bright matrixes are U-rich phases, based on the EDS analysis. The compositions are different, but all the U-rich phases should contain both α and γ phases, according to the XRD analysis.

The dark precipitates are found to be Zr-rich phases in the sample annealed at 948K, while in the samples annealed at 1023K and 1123K, they are either Zr-rich phases or Zr-Mo-Ti-compounds.

The composition of the Zr-Mo-Ti compounds in the samples annealed at 1023K and 1123K are almost the same, considering the precipitation size and the interaction volume. Therefore, they are named as a Zr-Mo-Ti-compound in both cases (Figure 7 and Figure 8). The composition of the Zr-rich phases is consistent regardless of the annealing temperature, so this phase is stable and does not change upon heating, at least to 1123K. The structures of the dark precipitates (Zr-rich phases or Zr-Mo-Ti-compounds) are not fully characterized because they cannot be detected with XRD.

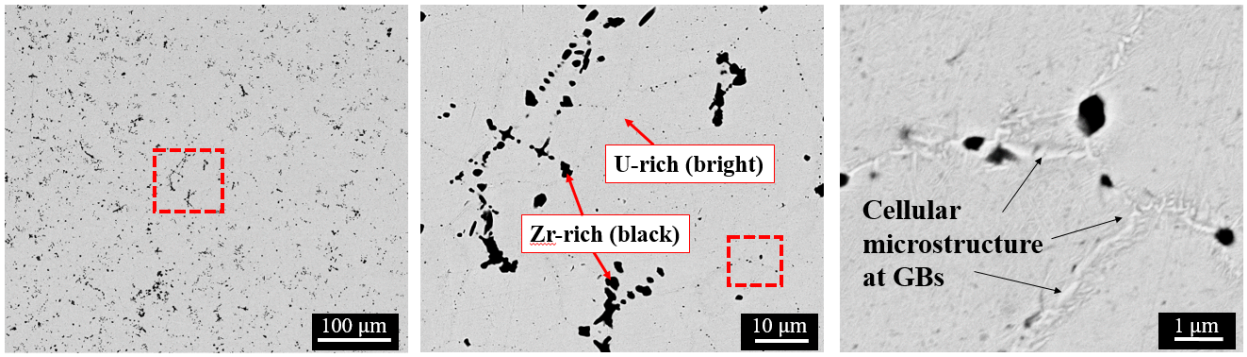

Figure 4. SEM/BSE micrographs for U-MT7Z DSC post-test sample: (a) is the overview image, (b) is the higher magnification image for the region indicated by the red rectangle in (a), (c) is the higher magnification image for the region indicated by the red rectangle in (b).

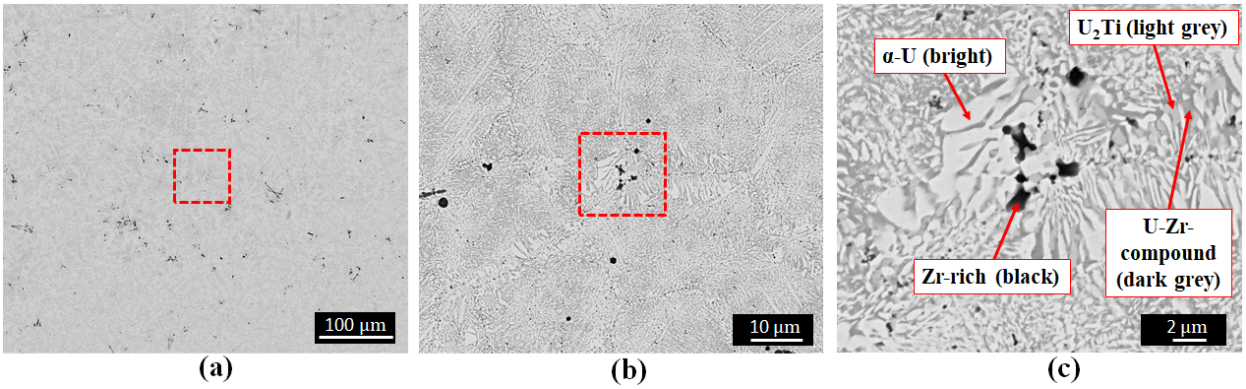

Figure 5. SEM/BSE micrographs for U-MT7Z annealed at 873K: (a) is the overview image, (b) is the higher magnification image for the region indicated by the red rectangle in (a), (c) is the higher magnification image for the region indicated by the red rectangle in (b).

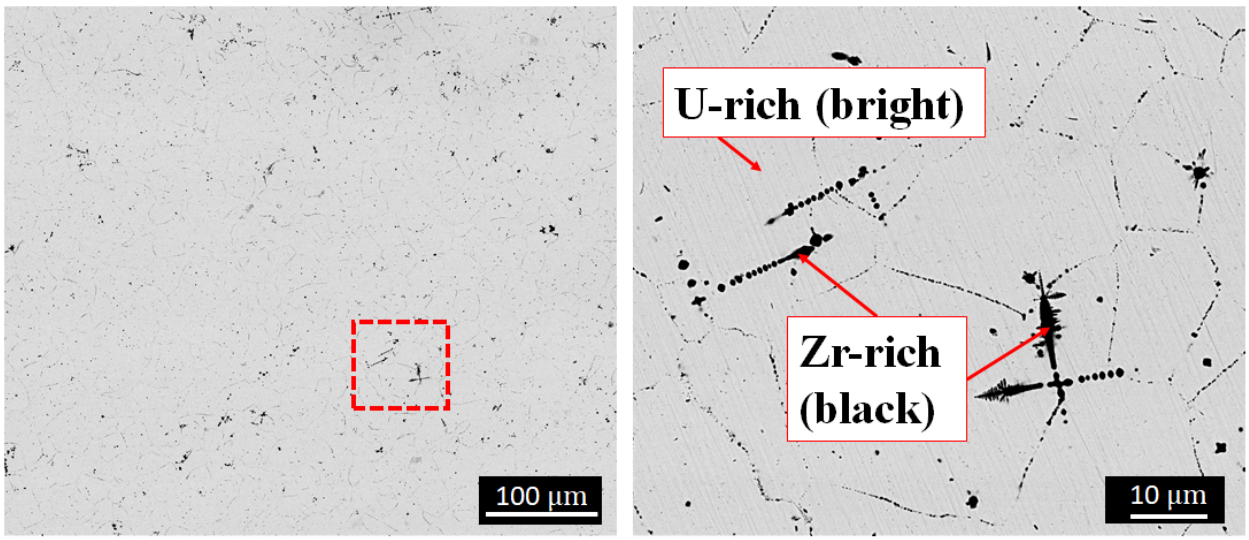

Figure 6. SEM/BSE micrographs for U-MT7Z annealed at 948K: (a) is the overview image, (b) is the higher magnification image for the region indicated by the red rectangle in (a).

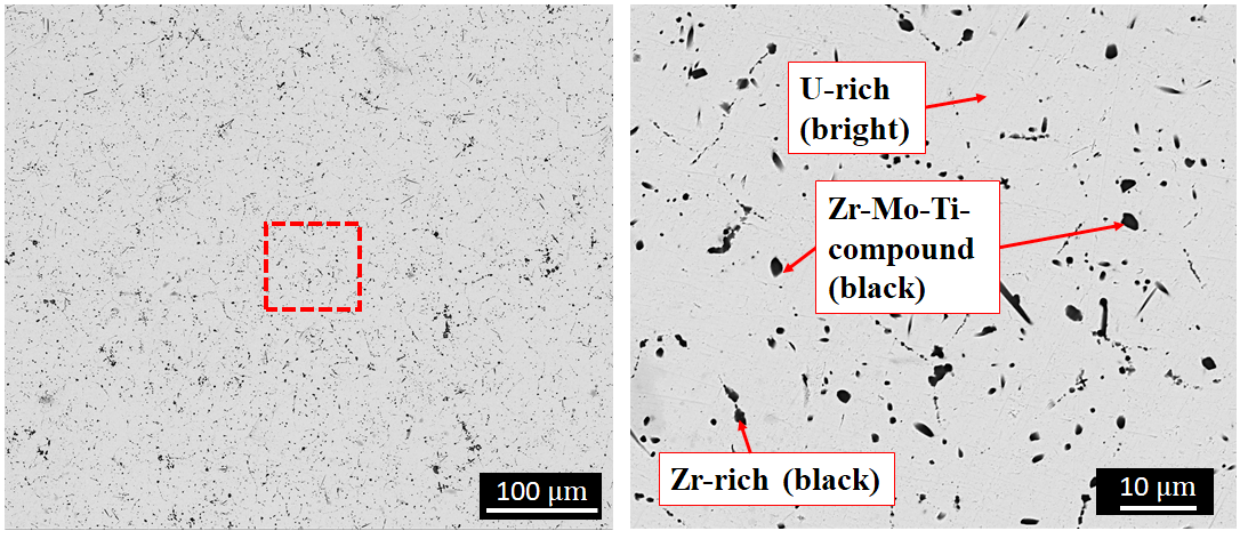

Figure 7. SEM/BSE micrographs for U-MT7Z annealed at 1023K: (a) is the overview image, (b) is the higher magnification image for the region indicated by the red rectangle in (a).

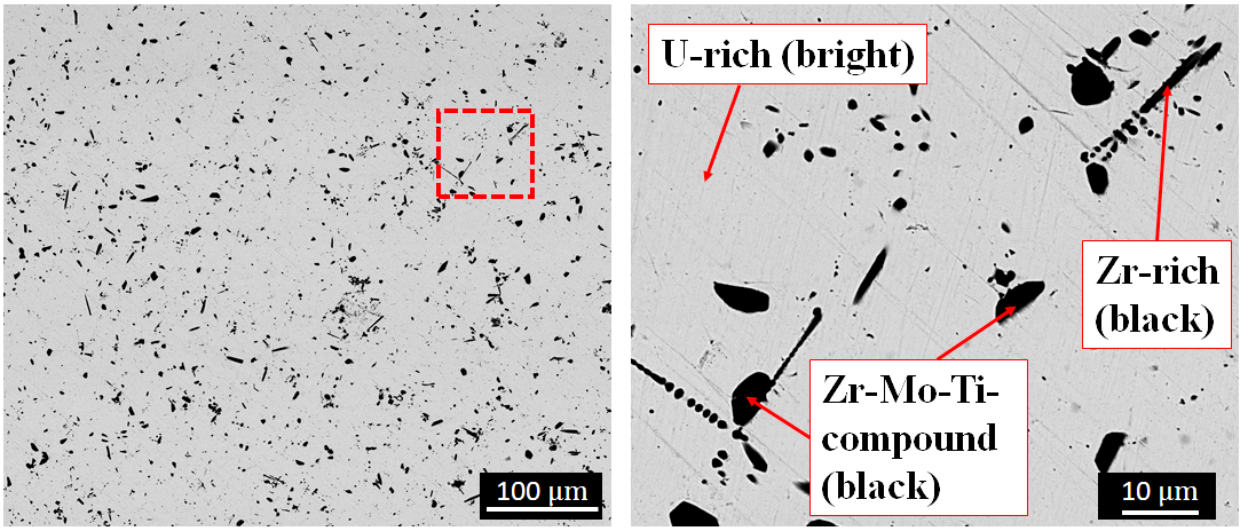

Figure 8. SEM/BSE micrographs for U-MT7Z annealed at 1123K: (a) is the overview image, (b) is the higher magnification image for the region indicated by the red rectangle in (a).

Table 4. Representative composition (at. %) of the phases in U-MT7Z alloys. The phases are indicated in the SEM images shown in Figure 4 to Figure 8.

Sample	Phase	U	Mo	Ti	Zr
DSC post-test (Figure 4)	U-rich	80	2	6	12
	Zr-rich	6	0	5	89
873K (Figure 5)	α-U	99	0	0	1
	U_2Ti	64	3	27	6
	U-Zr-compound	45	6	9	40
	Zr-rich	4	0	5	91
948K (Figure 6)	U-rich	79	2	6	13
	Zr-rich	9	0	4	87
1023K (Figure 7)	U-rich	84	2	7	6
	Zr-Mo-Ti-compound	10	12	12	66
	Zr-rich	7	0	5	88
1123K (Figure 8)	U-rich	74	5	8	13
	Zr-Mo-Ti-compound	1	17	10	72
	Zr-rich	4	1	5	90

3.2 U-MT5Z

3.2.1 DSC

An example of the DSC curve on U-MT5Z is shown in Figure 9a. There are two peaks observed, but they are overlapped. The overlapped peaks are separated after performing the peak fitting as shown in Figure 9b - Figure 9d. T_{onset}, T_{ext}, and T_{endset} are determined to be 881.0K, 907.2K,

917.2K for peak 1, and 889.6K, 984.3K, 1003.1K for peak 2. Other curves were analyzed using the same procedure, the data are summarized in Table 5.

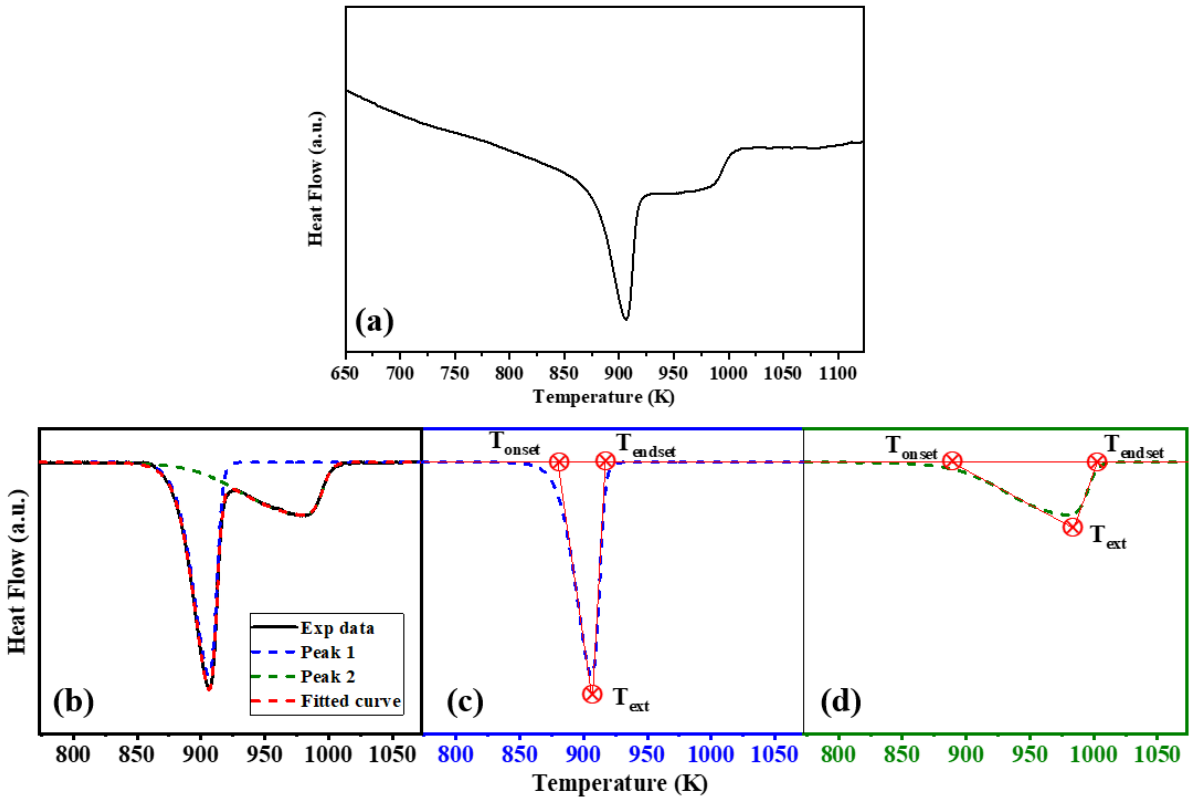

Figure 9. DSC analysis for U-MT5Z alloy: (a) an example of the DSC curve, (b) peak fitting, (c) peak 1, (d) peak 2.

Table 5. The peak data of as-cast U-MT5Z (unit: K).

	T_{onset}	T_{ext}	T_{endset}
Peak 1	876.3 ± 2.6	903.2 ± 2.5	913.4 ± 2.4
Peak 2	893.2 ± 8.3	981.0 ± 1.9	998.0 ± 3.1

3.2.2 XRD

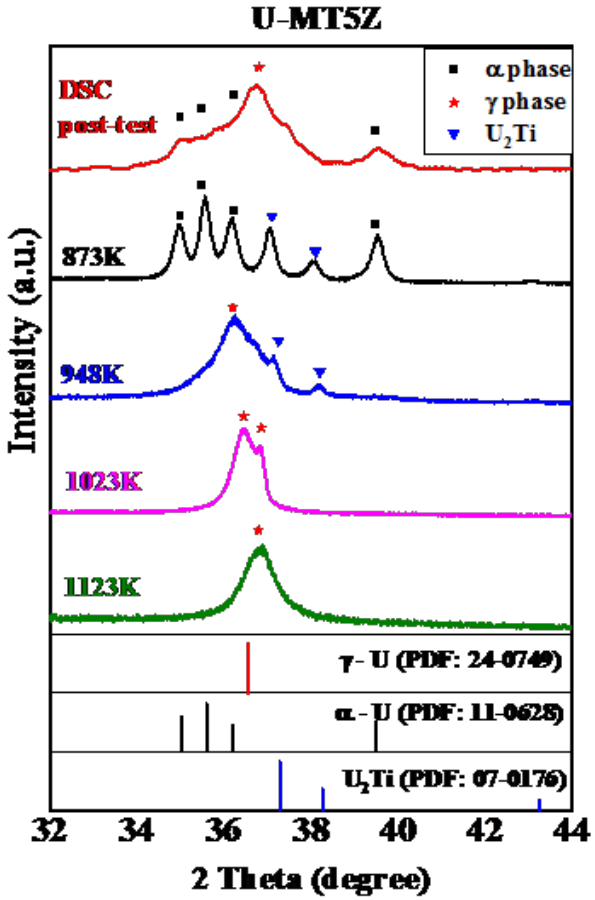

Figure 10. XRD results for U-MT5Z.

The XRD spectra for the U-MT5Z alloy are shown in Figure 10. In the DSC post-test sample, α and γ phases are observed. At 873K, α-U and U_2Ti are observed. At 948K, γ phase and U_2Ti are present. The U_2Ti intermetallic is no longer presented in the 1023K spectrum. The 1023K XRD spectrum has two peaks, although the second peak was not observed in the 948K spectrum. The γ phase peak in the 948K spectrum is broad, so the second peak may be present, but not resolved. These peaks collapse into a single peak in the 1123K spectrum. The presence of the two separated peaks in the 1023K spectrum suggests it is γ^0 phase in the sample.

In uranium alloys, the variants of γ-U are γ^s and γ^0 phases [20]. The γ^s phase might be interpreted as a doubled BCC cell in two directions due to periodic displacement of central atoms in the unit cells [20, 32]. Its XRD spectrum is similar to that of γ-U with the doubled lattice constant [32]. For the γ^0 phase, one of the distinguishable features is the two adjacent peaks [33,34]. As indicated by Ref.[34], the peak from γ phase splits into two adjacent peaks upon transforming into γ^0 phase. Therefore, the phase present in the sample annealed at 1023K is suggested to be γ^0 phase. Such phases have been reported in the U-Mo, U-Ti, U-Zr, and U-Mo-Ti systems [19]. The structure was found to be body-centered tetragonal (bct) [19], not bcc as in γ phase. The

difference is that the lattice parameter in γ^0 has the relation of due to the tetragonal structure while it is in γ due to the cubic structure [35]. This is a slight distortion in the cubic lattice, with the c/a ratio ~0.98.

A comparison can be made between U-MT7Z and U-MT5Z alloys. In the sample annealed at 948K/1023K/1123K, no α-phase was present in U-MT5Z. The difference is due to the different content of Mo, Ti, and Zr. The U-MT5Z alloy contains more Mo and Ti but less Zr. In the U-Mo system, 6 wt. % Mo is needed to retain the γ phase [36]. U-MT5Z only has 2.5 wt. % Mo, so there is a significant contribution from Zr and Ti. At 1023K, γ^0 phase is formed in U-MT5Z, while it is γ phase in U-MT7Z. In the U-Mo system, the formation of the γ^0 phase is related to the Mo concentration as this phase was found in the alloys with the Mo content ranging from 5 to 7 wt.% (or 11 to 15 at.%) [35, 33, 34].

The XRD results in both alloys (Figure 3 and Figure 10) show some deviation from the standard PDF peaks, especially for the γ phase.This should be due to the presence of the alloying elements Mo,Ti, and Zr in the γ phase. For instance, in the samples quenched from 948K, 1023K, and 1123K, the U-rich matrix is observed under SEM (Figure 13 to Figure 15), and it is suggested to be γ phase based on the XRD. According to the compositional analysis (Table 4 and Table 6), the U-rich matrix always have a small amount of the alloying elements Mo,Ti, and Zr. Those elements could be substitutional or interstitial (it is not clear in the current study though), but in either case it will cause the deviations in the lattice parameters and thus the shift in the peaks.

3.2.3 SEM/EDS

Representative BSE images for the U-MT5Z alloys are shown in Figure 11 to Figure 15, with the EDS analysis listed in Table 6. The EDS compositions listed are an average, as described for the U-MT7Z alloy. Compared to that of U-MT7Z alloys, the microstructure is very similar, but there are differences, as summarized:

1. The compositions measured by EDS analysis of the phases are different, due to the different Mo and Ti concentrations in the two alloys.
2. The cellular reactions are observed in both DSC post-test samples (marked in Figure 4c and Figure 11c). The difference is, the cellular reaction is observed associated with visible GBs in U-MT7Z (Figure 4c), while the GBs are not shown in U-MT5Z (Figure 11c).
3. In the U-MT5Z alloy annealed at 873K (Figure 12), the phases found are α-U, U_2Ti, and Zr-rich phases. The U-Zr compound which is observed in U-MT7Z alloy (Figure 5) is not found.
4. In the U-MT5Z alloy annealed at 948K (Figure 13), U_2Ti is found, in contrast to the U-MT7Z alloy (Figure 6). The corresponding XRD patterns (Figure 10) also support this. In addition, U_2Ti is found at the grain boundaries based on the SEM image.

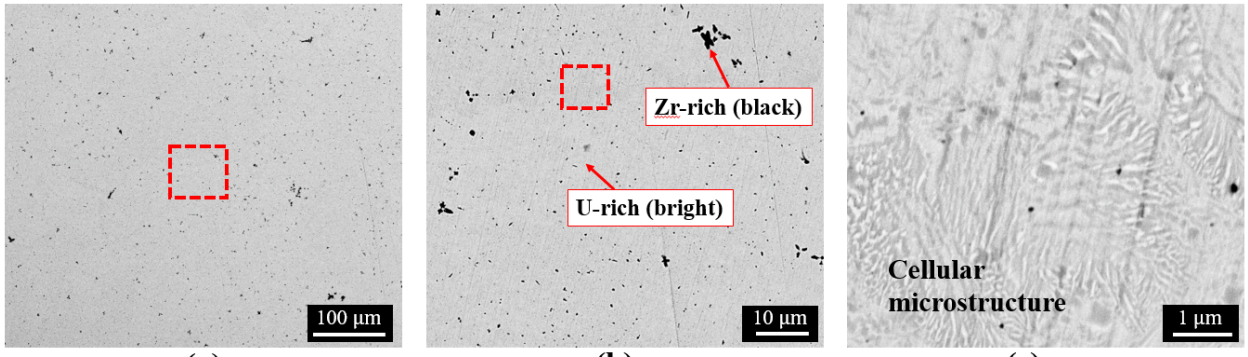

Figure 11. SEM/BSE micrographs for U-MT5Z DSC post-test sample: (a) is the overview image, (b) is the higher magnification image for the region indicated by the red rectangle in (a), (c) is the higher magnification image for the region indicated by the red rectangle in (b).

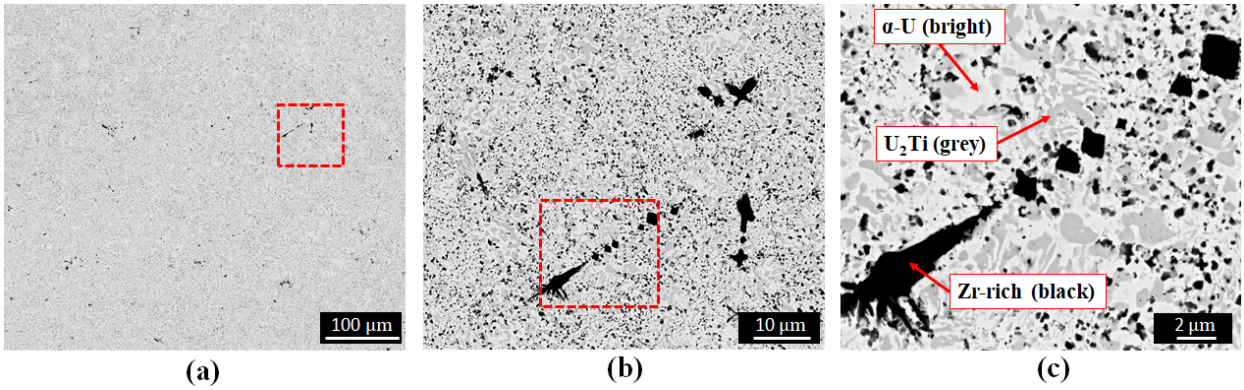

Figure 12. SEM/BSE micrographs for U-MT5Z annealed at 873K: (a) is the overview image, (b) is the higher magnification image for the region indicated by the red rectangle in (a), (c) is the higher magnification image for the region indicated by the red rectangle in (b).

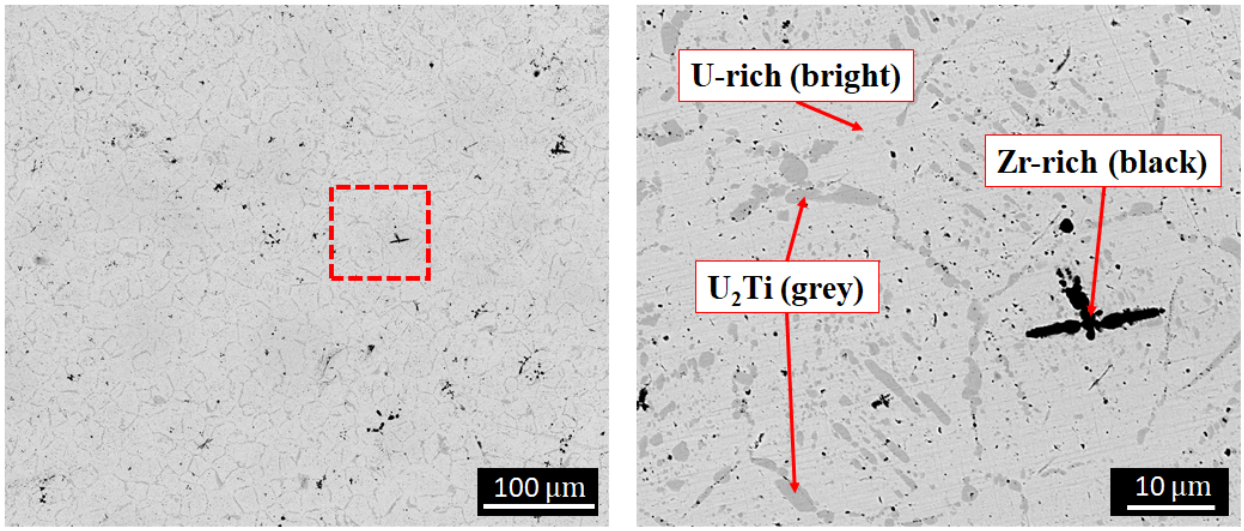

Figure 13. SEM/BSE micrographs for U-MT5Z annealed at 948K: (a) is the overview image, (b) is the higher magnification image for the region indicated by the red rectangle in (a).

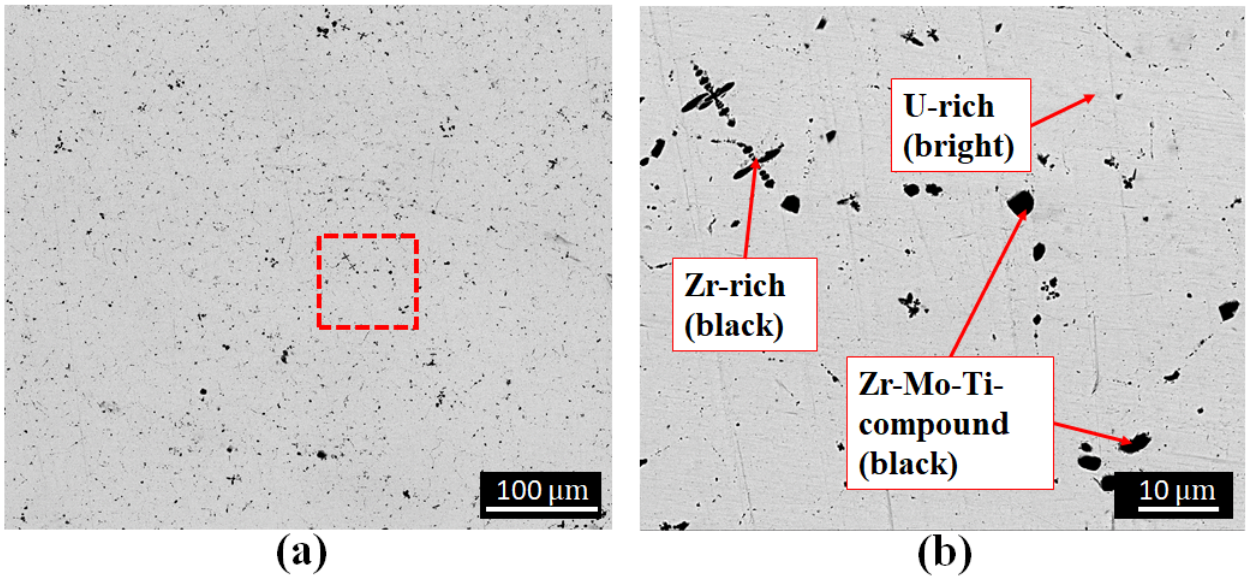

Figure 14. SEM/BSE micrographs for U-MT5Z annealed at 1023K: (a) is the overview image, (b) is the higher magnification image for the region indicated by the red rectangle in (a).

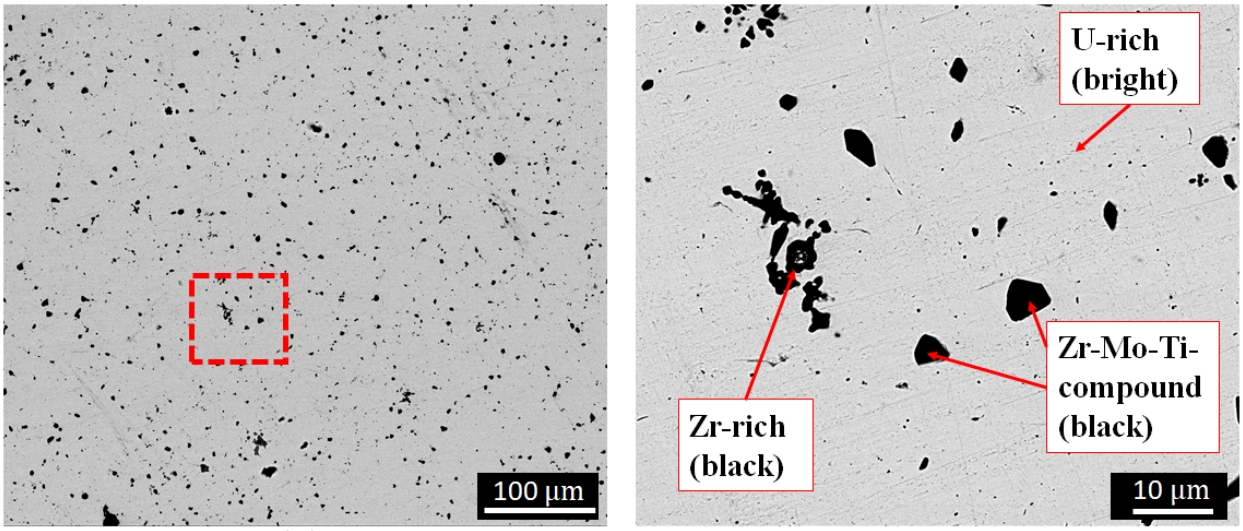

Figure 15. SEM/BSE micrographs for U-MT5Z annealed at 1123K: (a) is the overview image, (b) is the higher magnification image for the region indicated by the red rectangle in (a).

Table 6. Representative composition (at. %) of the phases for U-MT5Z. The phases are indicated in the SEM images shown in Figure 11 to Figure 15.

Sample	Phase	U	Mo	Ti	Zr
DSC post-test (Figure 11)	U-rich	78	4	9	9
	Zr-rich	2	1	9	88
873K (Figure 12)	α-U	100	0	0	0
	U_2Ti	63	3	28	6
	Zr-rich	2	2	8	88
948K (Figure 13)	U-rich	83	2	7	8
	U_2Ti	66	1	31	2
	Zr-rich	4	1	8	87
1023K (Figure 14)	U-rich	78	4	10	8
	Zr-Mo-Ti-compound	12	14	12	62
	Zr-rich*	12	1	9	78
1123K (Figure 15)	U-rich	76	5	12	7
	Zr-Mo-Ti-compound	1	16	14	69
	Zr-rich	3	1	9	87

* The 1023K sample has a higher U content in the Zr-rich as compared to the other samples, this is most likely because the Zr-rich precipitates in that corresponding figure (Figure 14b) are smaller than the others so the U content is higher due to the interaction volume.

4. Discussion

The phase transitions

For U-MT5Z alloy, the DSC curve shows two transition peaks. The starting phases are α and γ, as they are present in the post-test samples. The phases transform into γ phase as the first peak takes place, i.e., the first peak ascribes to α → γ transition. The transition starts at 876.3K indicated by T_{onset}, and finishes at 913.4K indicated by T_{endset}. U_2Ti are found in the samples annealed at 873K and 948K, but those samples were isothermally annealed for 72h. In the DSC test, the temperature was continually changed, so it is suggested that the formation of U_2Ti is a chemical reaction that will continue to happen during the DSC heating. At this point, no U_2Ti formation peak was identified in DSC curve. However, there is a second peak which should correspond to U_2Ti → γ. The transition starts at 893.2K (T_{onset}), and finishes at 998.0K (T_{endset}). This was verified by the annealing tests, U_2Ti are not present in the samples annealed at 1023K and 1123K, indicating that U_2Ti has already transformed into γ phase.

For U-MT7Z, the phase transition mechanism should be analogous to that of U-MT5Z, but there is only one peak observed in the DSC curve (Figure 2a), and the peak position is between the two peaks of U-MT5Z. It is suggested that the two transitions (i.e., α → γ and U_2Ti → γ) are merged into one peak. The different transition behaviors between the two alloys should due to the different compositions. Accordingly, the single transition observed in U-MT7Z ascribes to α + U_2Ti → γ. The transition starts at 894.3K (T_{onset}), and finishes at 926.5K (T_{endset}). After the transition, the alloy stays at γ phase. This indicates that the phases at 948K, 1023K and 1123K are the same (i.e., γ phase). In their XRD spectra (Figure 3), however, α phase is present. This can be due to the martensitic transformation. It is widely recognized that uranium alloys quenched from the γ phase may retain the γ phase or undergo a martensitic transformation [18]. If a martensitic transformation has taken place, α phase will form [18]. In order to retain the γ phase at room temperature, the alloying composition is one of the key factors. For example, in the U-Zr system, at least 11 wt. % Zr [37] is required, while in the U-Mo system at least 6 wt. % Mo is required [36] to retain the γ phase. U-10Zr quenched from the γ phase will undergo a martensitic transformation while U-10Mo will not. Available studies show that if the alloy contains more Mo, it is less likely to undergo martensitic transformations [33, 38]. U-MT7Z shows a martensitic transformation, while U-MT5Z does not, indicating enough Mo is present to retain the γ phase.

The γ onset temperatures

The purpose of lowering the γ onset temperature is because α phase is not desirable. α phase (for example, orthorhombic α-U) is not desirable because it shows poor dimensional stability under irradiation due to anisotropic growth and swelling [39, 40]. Hence, as long as α phase disappears the fuel will be in the favorable γ phase. In this work, it is determined that the onset temperature for γ phase is 894.3K for U-MT7Z, and 876.3K for U-MT5Z. As stated previously Mo lowers the onset temperature more than the other elements present, thus the decrease in γ phase onset temperature is due to the increase in Mo content. It is interesting to compare the data to the U-Mo binary system [7], as shown in Figure 16. In the alloys containing 90 wt.% uranium (U-1.5Mo-1.5Ti-7Zr, U-2.5Mo-2.5Ti-5Zr, and U-10Mo), the γ onset temperature decreases as the Mo content increases. In U-1.5Mo, the γ onset temperature is 828K [7]; while in

U-1.5Mo-1.5Ti-7Zr, the γ onset temperature is higher. The difference should be due to Ti/Zr. For the two alloys with 2.5 wt.% Mo, similar phenomenon is also observed.

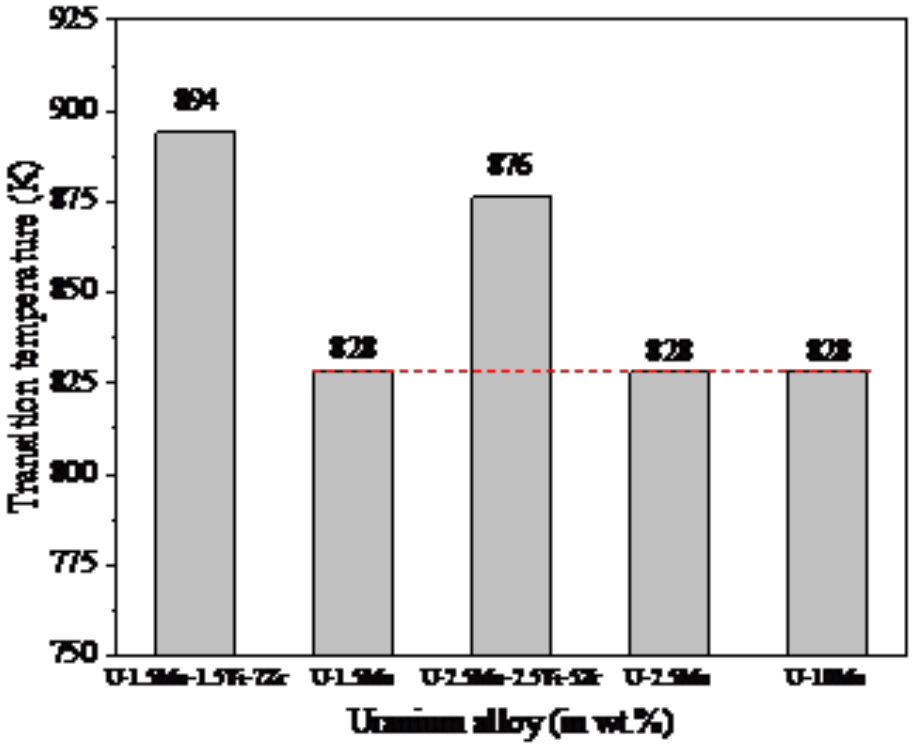

Figure 16. A comparison of the γ onset temperatures for Mo-containing uranium alloys. The red dash line is the eutectoid temperature in the U-Mo binary system [7] at the U-rich side. The U-rich side contains 66.7 to 99.9 at.% U (or > 83.2 wt.% U), alloys U-1.5Mo, U-2.5Mo, and U-10Mo are covered in this range.

5. Conclusion

In this work, the phase transitions of two quaternary fuel alloys (U-MT7Z and U-MT5Z) up to 1123K are investigated by combining DSC and XRD analyses. The phase transitions are different in the two UMTZ alloys primarily due to their different compositions. The single phase transition observed in the U-MT7Z alloy is $\alpha + U_2Ti \rightarrow \gamma$ with an onset temperature of 894K. In the U-MT5Z alloy, the phase transitions are $\alpha \rightarrow \gamma$ with an onset temperature of 876K, and $U_2Ti \rightarrow \gamma$ with an onset temperature of 893K. The γ phase onset temperature of U-MT5Z is lower than that of U-MT7Z due to the higher Mo content. With SEM, the microstructures are also investigated. It is observed that there are some minor phases changed in different annealed samples, but those changes are not detected by DSC or XRD.

The fuel alloys being investigated in the current work contain less Mo as compared to the previous studies because low Mo content is expected to reduce FCCI. However, the FCCI investigation is not present in this work. It is not clear if the Mo content of these alloys is low enough to significantly reduce FCCI, thus more investigation is needed. One effective method to

evaluate FCCI is diffusion couple tests. Relevant work will be performed in the future to investigate fuel cladding compatibilities under the temperatures of interest.

Acknowledgment

This work was supported through INL's Laboratory Directed Research & Development Program under DOE Idaho Operations Office Contract DE-AC07-05ID14517. Accordingly, the U.S. Government retains and the publisher, by accepting the article for publication, acknowledges that the U.S. Government retains a nonexclusive, paid-up, irrevocable, worldwide license to publish or reproduce the published form of this manuscript or allow others to do so, for U.S. Government purposes. The advice and help by Nanoscale Characterization and Fabrication Laboratory at Virginia Tech are also highly appreciated.

Reference

[1] J.M. Harp, D.L. Porter, B.D. Miller, T.L. Trowbridge, W.J. Carmack, Scanning electron microscopy examination of a Fast Flux Test Facility irradiated U-10Zr fuel cross section clad with HT-9, J. Nucl. Mater. (2017). doi:10.1016/j.jnucmat.2017.07.040.
[2] J.M. Harp, H.J.M. Chichester, L. Capriotti, Postirradiation examination results of several metallic fuel alloys and forms from low burnup AFC irradiations, 509 (2018) 377–391. doi:10.1016/j.jnucmat.2018.07.003.
[3] R.D. Mariani, D.L. Porter, S.L. Hayes, J.R. Kennedy, Metallic Fuels : The EBR-II legacy and recent advances, Procedia Chem. 7 (2012) 513–520. doi:10.1016/j.proche.2012.10.078.
[4] R.D. Mariani, D.L. Porter, J.R. Kennedy, S.L. Hayes, V.S. Blackwood, Z.S. Jones, D.L. Olson, B. Mishra, New Fuel Alloys Seeking Optimal Solidus and Phase Behavior for High Burnup and TRU Burning, IAEA, International Atomic Energy Agency (IAEA), 2015. http://www-pub.iaea.org/MTCD/Publications/PDF/SupplementaryMaterials/P1665CD/Track5_Fuels.pdf.
[5] J. Harp, L. Capriotti, F. Cappia, Postirradiation examination of recently irradiated metallic fuel concepts, (2018). https://inldigitallibrary.inl.gov/sites/sti/sti/Sort_8542.pdf.
[6] Y. Park, N. Eriksson, R. Newell, D.D. Keiser, Y.H. Sohn, Phase decomposition of γ-U (bcc) in U-10 wt% Mo fuel alloy during hot isostatic pressing of monolithic fuel plate, J. Nucl. Mater. 480 (2016) 271–280. doi:10.1016/j.jnucmat.2016.08.022.
[7] H. Okamoto, Mo-U (Molybdenum-Uranium), J. Phase Equilibria Diffus. (2012). doi:10.1007/s11669-012-0095-z.
[8] H. Okamoto, Nb-U (Niobium-Uranium), J. Phase Equilibria Diffus. 30 (2009) 411. doi:10.1007/s11669-009-9543-9.
[9] R.I. Sheldon, D.E. Peterson, The U-Zr (Uranium-Zirconium) system, Bull. Alloy Phase Diagrams. (1989). doi:10.1007/BF02881432.
[10] H. Okamoto, Ti-U (Titanium-Uranium), J. Phase Equilibria Diffus. 34 (2013) 61–62. doi:10.1007/s11669-012-0127-8.
[11] C.T. Howard, The Behavior of Palladium as A Getter for Lanthanide Fission Products in U-Mo-Ti-Zr Fast Reactor Fuels, Colorado School of Mines (2017).
[12] V.S. Blackwood, As-cast uranium-molybdenum based metallic fuel candidates and the effects of carbon addition, Colorado School of Mines (2014).

[13] W. Zhuo, Y. Xie, M.T. Benson, J. Ge, R.D. Mariani, J. Zhang, XRD and SEM/EDS characterization of two quaternary fuel alloys (U-2.5Mo-2.5Ti-5.0Zr and U-1.5Mo-1.5Ti-7.0Zr in wt%) for fast reactors, Mater. Charact. (2020) 110696. doi:https://doi.org/10.1016/j.matchar.2020.110696.
[14] D.R. Lide, CRC handbook of chemistry and physics, CRC press (2004).
[15] M. Rodríguez Chialanza, I. Sierra, A. Pérez Parada, L. Fornaro, Identification and quantitation of semi-crystalline microplastics using image analysis and differential scanning calorimetry, Environ. Sci. Pollut. Res. (2018). doi:10.1007/s11356-018-1846-0.
[16] W.J. Boettinger, U.R. Kattner, K.-W. Moon, J.H. Perepezko, DTA and Heat-Flux DSC Measurements of Alloy Melting and Freezing, 2006. doi:10.1016/B978-008044629-5/50005-7.
[17] https://thermalmaterials.org/wiki-pcm/onset-temperature
[18] S. Irukuvarghula, S. Ahn, S.M. McDeavitt, Decomposition of the γ phase in as-cast and quenched U-Zr alloys, J. Nucl. Mater. 473 (2016) 206–217. doi:10.1016/j.jnucmat.2016.02.028.
[19] H.L. Yakel, A review of x-ray diffraction studies in uranium alloys, Oak Ridge, Tennessee 37830, 1974.
[20] A. Landa, P. Söderlind, A. Wu, Phase stability in U-6Nb alloy doped with ti from the first principles theory, Appl. Sci. 10 (2020). doi:10.3390/app10103417.
[21] S. Kaity, J. Banerjee, S.C. Parida, P.G. Behere, V. Bhasin, Structural, microstructural and thermal analysis of U−(6-x)Zr−xMo alloys (x = 0, 2, 4, 6), J. Nucl. Mater. 532 (2020) 152046. doi:10.1016/j.jnucmat.2020.152046.
[22] S. Jana, N. Overman, T. Varga, C. Lavender, V. V. Joshi, Phase transformation kinetics in rolled U-10 wt. % Mo foil: Effect of post-rolling heat treatment and prior γ-UMo grain size, J. Nucl. Mater. (2017). doi:10.1016/j.jnucmat.2017.09.030.
[23] S. Jana, A. Devaraj, L. Kovarik, B. Arey, L. Sweet, T. Varga, C. Lavender, V. Joshi, Kinetics of cellular transformation and competing precipitation mechanisms during sub-eutectoid annealing of U10Mo alloys, J. Alloys Compd. (2017). doi:10.1016/j.jallcom.2017.06.292.
[24] J.T. McKeown, S. Irukuvarghula, S. Ahn, M.A. Wall, L.L. Hsiung, S. McDeavitt, P.E.A. Turchi, Coexistence of the α and δ phases in an as-cast uranium-rich U-Zr alloy, J. Nucl. Mater. (2013). doi:10.1016/j.jnucmat.2013.01.313.
[25] Y. Zhang, X. Wang, G. Zeng, H. Wang, J. Jia, L. Sheng, P. Zhang, Microstructural investigation of as-cast uranium rich U-Zr alloys, J. Nucl. Mater. (2016). doi:10.1016/j.jnucmat.2016.01.005.
[26] W. Zhuo, Y. Xie, M.T. Benson, Q. Yang, R.D. Mariani, J. Zhang, Experimental investigation of FCCI using diffusion couple test between UZr fuel with Sb additive and cladding, Nucl. Sci. Eng. (2020). doi:10.1080/00295639.2020.1713656.
[27] C.L. Trybus, J.E. Sanecki, S.P. Henslee, Casting of metallic fuel containing minor actinide additions, J. Nucl. Mater. 204 (1993) 50–55. doi:10.1016/0022-3115(93)90198-8.
[28] D.E. Janney, T.P.O. Holleran, Zr Inclusions in Actinide – Zr alloys : new data and ideas about how they form, J. Nucl. Mater. 460 (2015) 13–15. doi:10.1016/j.jnucmat.2015.01.065.
[29] D.E. Janney, J.R. Kennedy, J.W. Madden, T.P. O'Holleran, Crystal structure of high-Zr inclusions in an alloy containing U, Pu, Np, Am, Zr and rare-earth elements, J. Nucl. Mater. 448 (2014) 109–112. doi:10.1016/j.jnucmat.2014.01.044.
[30] S. Ahn, Comprehensive investigation of the uranium-zirconium alloy system: thermophysical properties, Phase Characterization and Ion Implantation Effects, Texas A&M University, 2013.

[31] W. Zhuo, Y. Xie, M.T. Benson, Q. Yang, R.D. Mariani, J. Zhang, Experimental Investigation of FCCI Using Diffusion Couple Test Between UZr Fuel with Sb Additive and Cladding, Nucl. Sci. Eng. 194 (2020) 462–476. doi:10.1080/00295639.2020.1713656.
[32] S. V. Starikov, L.N. Kolotova, A.Y. Kuksin, D.E. Smirnova, V.I. Tseplyaev, Atomistic simulation of cubic and tetragonal phases of U-Mo alloy: Structure and thermodynamic properties, J. Nucl. Mater. 499 (2018) 451–463. doi:10.1016/j.jnucmat.2017.11.047.
[33] N.T.H. Kim-Ngan, I. Tkach, S. Mašsková, L. Havela, A. Warren, T. Scott, Cubic γ-phase U-Mo alloys synthesized by splat-cooling, Adv. Nat. Sci. Nanosci. Nanotechnol. 4 (2013). doi:10.1088/2043-6262/4/3/035006.
[34] M.J. Lehmann, R.F. Hills, Proposed nomenclature for phases in uranium alloys, J. Nucl. Mater. 2 (1960) 261–268. doi:10.1016/0022-3115(60)90060-x.
[35] I. Tkach, N.T.H. Kim-Ngan, S. Mašková, M. Dzevenko, L. Havela, A. Warren, C. Stitt, T. Scott, Characterization of cubic γ-phase uranium molybdenum alloys synthesized by ultrafast cooling, J. Alloys Compd. 534 (2012) 101–109. doi:10.1016/j.jallcom.2012.04.028.
[36] Y.S. Kim, Uranium Intermetallic Fuels (U–Al, U–Si, U–Mo), in: R.J.M.B.T.-C.N.M. Konings (Ed.), Compr. Nucl. Mater., Elsevier, Oxford, 2012: pp. 391–422. doi:https://doi.org/10.1016/B978-0-08-056033-5.00112-9.
[37] D.E. Janney, S.L. Hayes, Experimentally Known Properties of U-10Zr Alloys: A Critical Review, Nucl. Technol. 203 (2018) 109–128. doi:10.1080/00295450.2018.1435137.
[38] J.G. Speer, D. V Edmonds, An investigation of the γ → α martensitic transformation in uranium alloys, Acta Metall. 36 (1988) 1015−1033. doi:https://doi.org/10.1016/0001-6160(88)90156-3.
[39] J.H. Kittel, B.R.T. Frost, J.P. Mustelier, K.Q. Bagley, G.C. Crittenden, J. Van Dievoet, History of fast reactor fuel development, J. Nucl. Mater. (1993). doi:10.1016/0022-3115(93)90193-3.
[40] M.K. Meyer, J. Gan, J.F. Jue, D.D. Keiser, E. Perez, A. Robinson, D.M. Wachs, N. Woolstenhulme, G.L. Hofman, Y.S. Kim, Irradiation performance of U-Mo monolithic fuel, Nucl. Eng. Technol. (2014). doi:10.5516/NET.07.2014.706.